Multipole surface-plasmon modes on simple metals

Jordi Sellarès and Nuria Barberán
Departament d'Estructura i Constituents de la Matèria, Facultat de Física, Universitat de Barcelona, E-08028 Barcelona, Spain
(Received 20 December 1993)

The average multipole surface-plasmon energy for simple metals, as well as that of ordinary surface and bulk plasmons, is obtained using energy-weighted moments of the electronic response to sufficiently general external perturbations. A local approximation of exchange and correlation effects is used within a jellium model. Band-structure effects are incorporated through an effective electronic mass. Taking advantage of the transparency of the method, we analyze under what circumstances such modes might be observable. It is shown that due to an interplay between Coulomb and kinetic energies, the multipole modes become unobservable for increasing values of the transferred momentum (q) parallel to the surface. The value of q at which the multipole mode becomes unobservable is much smaller than the cutoff value for Landau damping. The effect of the electronic surface diffuseness is also analyzed. We compare our results with previous density-functional calculations and with recent experimental data for Na, K, and Cs.

I. INTRODUCTION

Despite the great amount of theoretical effort invested in the characterization and understanding of multipole plasmon modes on metal surfaces,[1-8] and the existence of some indirect experimental signs in surface photoemission from Al (Ref. 9) and photoyield data from alkali metals,[10] direct experimental evidence has not been reported until recently in inelastic reflection electron scattering on smooth films of Na, K, and Cs.[11,12] Up to now , no experimental observation has been reported of the existence of these modes from energy-loss spectroscopy on high-density metals such as aluminum and still some uncertainties concerning their nature and properties are unsolved.

Multipole plasmon modes are associated with electronic-density fluctuations that are peaked at the surface region and have decreasing oscillating amplitude towards the interior of the metal. The integral of the electronic density perpendicular to the surface is zero.[8,12] Although these modes have a surface origin, they carry momentum both in the normal as well as in the parallel directions, making them optically active in contrast to ordinary surface plasmons, which have a monopole character. The frequency of the multipole mode lies, for a fixed value of the momentum q parallel to the surface, between the bulk and the monopole plasmon values. At $q=0$, both experimental data and theoretical calculations[12] intersect at approximately $0.8w_p$. This value of w is between the bulk and the surface values (w_p and $w_p/\sqrt{2}=0.71w_p$, respectively).

For small q values, the slope of the dispersion relation is positive as a consequence of the induced electronic-charge distribution. The centroid of the induced electronic charge, defined as

$$d(w)=\frac{\int dz\, z\delta n(z,w)}{\int dz\, \delta n(z,w)}\ , \tag{1}$$

where the induced charge δn is, in general, a complex function,[12] lies in the interior of the metal in contrast to the case of the centroid of ordinary surface modes, which lies outside and has a negative slope. As was discussed by Feibelman[7] and Tsuei *et al.*[11] in the long-wavelength limit, the energy of the mode depends on the average ground-state (g.s.) electronic density seen by the electrostatic potential created by the induced charge. The induced potential is peaked at the centroid position and as q increases becomes more localized in the region of the centroid, thus making the slope of the dispersion relation positive because of the increase of the average electronic density. There is no known analytical expression for the dispersion relation in the low-q limit.

The first theoretical predictions were developed within the hydrodynamical approximation,[1,2] which turned out to be able to obtain the new modes if a surface electronic structure, which mimicked the electronic-surface diffuseness, was assumed. Such modes disappear if a sharp metal-vacuum interface is assumed. Dobson and Harris[6] confirmed the existence of additional surface-plasmon modes on a bare jellium surface within a microscopic calculation and emphasized the use of a correctly self-consistent zero-order surface electron-density profile. Feibelman[7] and later Liebsch[8] obtained the response of the surface characterized by the centroid of the charge induced by time-dependent arbitrary external fields. The imaginary part of this frequency-dependent centroid function develops a resonant structure at about $0.8w_p$, which is due to the multipole normal mode. Within a time-dependent density-functional approach (TDLDA), Tsuei *et al.*[12] obtained good agreement with experimental data. In their calculation they emphasize the consistent treatment of the electron-electron interaction in the g.s. and in the dynamical response to an external perturbation.

The aim of the present work is to investigate some properties of the collective multipole excitations that have not been handled in previous studies, taking advan-

0163-1829/94/50(3)/1879(9)/$06.00

tage of the facilities of the sum-rule (SR) method used. The SR provides a useful approximation of the average excitation energies of fermion systems confined to different geometries. It has produced a wealth of information about the nature of collective modes in metallic systems.[13–19] Exchange and correlation can be easily incorporated within a local-density approximation and band effects can be included in a jellium model through an effective electronic mass. We pay special attention to the different contributions to the energy and address the question of under what circumstances such modes might be observable.

In the calculation we closely follow some previous works[16,19] and will only remark on the new points included in the present case. This paper is organized as follows. In Sec. II, the SR calculation is performed and compared with previous formulations carried out on different systems using the same technique. In Sec. III, results are compared with experimental data and previous theoretical calculations, and in Sec. IV, we present some concluding remarks.

II. GENERAL EQUATIONS

The SR approximation used in this work provides a method of obtaining the average excitation of a system in response to a given external operator, and it is especially useful when the system develops a dominantly collective response. SR's are energy moments of the strength function (also called the response function) $S(E)$ defined as

$$S(E)=\sum_l \delta(E-E_l)|\langle l|Q|0\rangle|^2 , \tag{2}$$

where the sum extends over all excited states. Q is the perturbing operator, E_l, $|l\rangle$, and $|0\rangle$ are the excitation energies, excited state, and the g.s. of the system, respectively. If by definition, the p-sum rule reads

$$m_p=\int E^p S(E)dE=\sum_l E_l^p|\langle l|Q|0\rangle|^2 , \tag{3}$$

the average value of the excitation energy and the variance σ^2 are given by

$$\bar{E}=m_1/m_0 , \tag{4}$$

$$\sigma^2=m_2/m_0-(m_1/m_0)^2 . \tag{5}$$

Among these moments, the ones with $p=-1$, 1, and 3 play an important role in the application of SR's to the study of collective resonance states of the system. They can be used to estimate $\bar{E}$ and σ^2. Defining $E_p=(m_p/m_{p-2})^{1/2}$, it has been shown[20] that

$$E_1\le\bar{E}\le E_3 , \tag{6}$$

$$\sigma^2\le(E_3^2-E_1^2)/4 . \tag{7}$$

If the external operator Q has the appropriate symmetry and couples to the normal modes of the system, then the response saturates by a single mode and most of the strength is in a narrow energy region. Under such conditions, as is the case for some resonant collective states, E_1 and E_3 are close together and both are good estimates of $\bar{E}$. We will concentrate on E_3 (the upper bound to the energy) from which good results have been obtained in previous works.[16,18,19] The dispersion relation will be obtained from

$$E_3=[m_3/m_1]^{1/2} . \tag{8}$$

Manipulation of Eq. (3) for $p=1$ and 3 leads[20,21] to simplified expressions that depend only on the Hamiltonian of the system, its g.s., and the external operator. These are given by

$$m_1=\tfrac{1}{2}\langle 0|[Q^\dagger,[H,Q]]|0\rangle , \tag{9}$$

and

$$m_3=\tfrac{1}{2}\langle 0|[[[Q^\dagger,H],[H,[H,Q]]]|0\rangle , \tag{10}$$

where $Q^\dagger$ denotes the Hermitian conjugate operator. The linear-energy moment m_1 is easily calculated from Eq. (9) when Q depends only on position. The cubic moment is easier to obtain by scaling the g.s. $|0\rangle$. Defining the scaled function as

$$|\eta\rangle=e^{\eta[H,Q]}|0\rangle , \tag{11}$$

we get

$$m_3=\frac{1}{2}\frac{\delta^2}{\delta\eta^2}\langle\eta|H|\eta\rangle\Big|_{\eta=0} . \tag{12}$$

We define the scaled particle and kinetic-energy densities [we use atomic units (a.u.) throughout]

$$n_\eta(\mathbf{r})=\langle\eta|\hat{n}|\eta\rangle=n+\eta n_1+\eta^2 n_2+\cdots , \tag{13}$$

$$\sigma_\eta(\mathbf{r})=\langle\eta|\hat{\sigma}|\eta\rangle=\sigma+\eta\sigma_1+\eta^2\sigma_2+\cdots , \tag{14}$$

where

$$\hat{n}=\sum_i \delta(\mathbf{r}-\mathbf{r}_i) , \tag{15}$$

$$\hat{\sigma}=\sum_i \overleftarrow{\nabla}_i\delta(\mathbf{r}-\mathbf{r}_i)\vec{\nabla}_i , \tag{16}$$

and

$$n=\langle 0|\hat{n}|0\rangle , \tag{17}$$

$$n_1=\langle 0|[\hat{n},[H,Q]]|0\rangle , \tag{18}$$

$$n_2=\tfrac{1}{2}\langle 0|[[\hat{n},[H,Q]],[H,Q]]|0\rangle , \tag{19}$$

with similar expressions for σ, σ_1, and σ_2. Notice that our particle and kinetic-energy densities are defined as

$$n=\sum_i|\phi_i|^2 , \tag{20}$$

$$\sigma=\sum_i|\vec{\nabla}\phi_i|^2 . \tag{21}$$

Expanding the expectation value of the Hamiltonian in powers of η, Eq. (12) provides a straightforward but cumbersome evaluation of m_3.

For r-dependent operators Q it has been shown[22] that σ_1 does not contribute to m_3 and that

$$n_1=-\nabla_i(nu_i) , \tag{22}$$

$$n_2=-\tfrac{1}{2}\nabla_i(n_1u_i)\ , \tag{23}$$

and

$$\sigma_2=\tfrac{1}{3}\sigma\{-u_k(\nabla_k\nabla_iu_i)+(\nabla_ju_i)[\nabla_iu_j+\nabla_ju_i]\}$$
$$+\tfrac{1}{4}(\nabla_i\nabla_ju_j)[\nabla_i\nabla_k(nu_k)]$$
$$+\tfrac{1}{4}(\nabla_in)(\nabla_j\nabla_ku_k)[\nabla_iu_j+\nabla_ju_i]\ , \tag{24}$$

where ∇_i means the Cartesian i-coordinate derivative, a sum over repeated indices is understood and

$$\mathbf{u}=\vec{\nabla}Q\ . \tag{25}$$

We refer the interested reader to Ref. 16 and references therein for further details.

The most accurate application of the method consists in the use of the self-consistent g.s. calculated from the same Hamiltonian H as that used in the determination of m_1 and m_3 in Eqs. (9) and (12). Instead, we use different analytical approximations of the g.s. We will show in the next section that the sensitivity of the results on the choice of the g.s. is extremely low.

The jellium model is used to describe the neutralizing positive background. The metal occupies the negative part of the z axis and $z=0$ is the position of the positive jellium edge. The Hamiltonian consists of a kinetic term (T), a direct Coulomb term (C), which includes electron-electron and electron-jellium interactions, as well as both an exchange (ex) and a correlation (cor) term.

For the exchange and correlation energy densities, Slater- and Wigner-type local expressions are used,

$$e(\mathrm{ex})=-\frac{3}{4}\left[\frac{3}{\pi}\right]^{1/3}n^{4/3} \tag{26}$$

and

$$e(\mathrm{cor})=-\frac{a(4\pi n/3)^{1/3}n}{b(4\pi n/3)^{1/3}+1}\ , \tag{27}$$

respectively, where n is the electron-density operator, $a=0.44$, and $b=7.8$. The use of other state-of-the-art representations of the local correlation energy, such as those of Refs. 23 and 24, does not change the numerical results by more than a few percent.[17] We stress that a different treatment has been followed with the kinetic term. The kinetic contribution to m_1 and m_3 has been evaluated using the one-body kinetic-energy operator of Eq. (16) in Eq. (12), which finally yields an expression that depends on the g.s. electronic and kinetic-energy densities [see Eq. (24)]. For this last density, the improved Thomas–Fermi–von Weizsäcker functional given by

$$\tau=\tfrac{3}{10}(3\pi^2)^{2/3}n^{5/3}+\frac{\beta}{8}\frac{n'^2}{n} \tag{28}$$

is used, where β is the von Weizsäcker coefficient (taken equal to $\frac{1}{2}$) and n' denotes the z derivative. As a consequence, the kinetic contribution contains nonlocality in contrast to the exchange and correlation terms that are purely local.

Once the Hamiltonian is fixed, the key part of the method lies in the election of an appropriate external operator Q; it must not mix nor miss the eigenmodes of the system. In previous works using the same method and the same Hamiltonian in the study of the normal modes of metallic spheres, two different operators were used. The first, $Q_s^{\mathrm{sph}}=r^lY_{l0}(\theta,\phi)$,[15] where $Y_{l0}(\theta,\phi)$ is the spherical harmonic function, provided the mean energy of the surface-plasmon excitations characterized by the well-defined quantum number l and the dispersion relation (energy versus radius of the sphere). The dispersion relation obtained agreed with previous calculations and with experimental data. A second operator, $Q_b^{\mathrm{sph}}=j_l(rq_r)Y_{l0}(\theta,\phi)$,[16] where j_l is the spherical Bessel function, added a new parameter q_r (momentum along the radial direction). This operator allowed the possibility of excitation of modes throughout the volume of the sphere. The induced density is peaked at the surface region but has decreasing amplitude oscillations towards the interior of the sphere. The spectrum turns out to be much richer than in the case of the first operator and for each l value, an extra index is necessary to specify the eigenmode. Due to the finite size of the sphere, the q_r momentum is quantized and only for some q_r values, related to the radius R of the sphere, the response has a resonant behavior, which yields an oscillatory structure to the energy of the system as a function of q_r (see Fig. 5 in Ref. 16).

Recently, the plane metallic surface has been examined using this same approximation.[19,25] The operator used to generate surface plasmons is $Q_s=e^{i\mathbf{q}\cdot\boldsymbol{\rho}}e^{qz}$, where $\mathbf{r}=(\boldsymbol{\rho},z)$. The well-defined quantum number is the momentum $\mathbf{q}$ parallel to the surface and the exponentially decreasing behavior inside the metal guarantees the convergence of the space integrals in the calculation.

For potassium the agreement with experimental data is quite good, comparable with other self-consistent theoretical calculations.[12] However, for Na this agreement diminishes for large q values.

The operator Q_{mp} capable of generating the multipole surface-plasma modes must fulfill several conditions. One of these conditions is that it must depend on an extra parameter (τ), momentum of a standing wave in the z direction. Furthermore, to generate extended modes in the volume with a non-negligible probability, the external operator must be peaked within the metal. The function chosen is

$$Q_{\mathrm{mp}}=e^{i\mathbf{q}\cdot\boldsymbol{\rho}}e^{-q^2z^2}\cos(\tau z)\ . \tag{29}$$

[The q component of the Fourier transform of the potential created by a point charge moving parallel to the surface at $z=0$ would be $Q=(1/2\pi q)e^{i\mathbf{q}\cdot\boldsymbol{\rho}}e^{-q|z|}$.]

A quite common criticism of this procedure is that one loses the physical meaning of the Q operator. The answer to this objection is that, in general, the energies of the normal modes of the system do not depend on the way one excites them. The main problem arises from the possible mixture of modes caused by Q. However, if the response is dominated by a collective mode, the structure of $S(E)$ in Eq. (2) has only one peak, the summation in Eq. (3) has only one term, and the contribution of Q to E_3

in Eq. (8) is completely eliminated. This is the case in the low-q-value region of the spectrum, but it is only approximate for increasing values of q. Other operators, which were easier to manage analytically, were tested, but either they did not show a sensitive resonant behavior of the energy as a function of τ, as we expected, or they did not correctly reproduce the limits for low q and τ values.

Using Eqs. (26)–(28) and (29) into Eqs. (9) and (12) yields integral expressions on the g.s. electronic density $n(z)$ along the z axis. The expressions for m_1 and m_3 are given in the Appendix. An effective electronic mass has been included to incorporate band effects.

Two different analytical approximations are used for $n(z)$; the first, a double-step function centered at $z=0$,

$$n_S(z)=\frac{n_0}{2}\left[\theta\left[-z-\frac{d}{2}\right]+\theta\left[-z+\frac{d}{2}\right]\right], \tag{30}$$

where $n_0=3/4\pi r_s^3$ (where r_s is the bulk one-electron radius), $\theta(x)$ is the step function, and d is the width of the electronic-profile step of density $n_0/2$. The second is an analytical approximation of the Lang-Kohn calculation given by

$$n_{\mathrm{LK}}(z)=\frac{n_0}{e^{z/\delta}+1}\ . \tag{31}$$

The double step is taken to be the surface width of the smooth density [Eq. (31)], defined as $d=z_2-z_1$ where $n(z_2)=0.1n_0$, and $n(z_1)=0.9n_0$.[19]

The effective electron mass used in the calculations and the δ parameter, which determines the softness of the electronic profile [Eq. (31)], are taken from the fit of the polynomial approximation to the experimental data given in Ref. 12 for the surface monopole modes and the analytical expression obtained using Q_s in the low-q limit, which is given by[19]

$$w(q)=\frac{w_p}{\sqrt{2m^*}}[1-q\delta\ln(2)]\ . \tag{32}$$

Numerical calculation of the space integrals is carried out along a longitude centered at $z=0$ and bounded by z values that satisfy the condition

$$e^{-2q^2z^2}\leq 10^{-10}\ , \tag{33}$$

for each q value. This exponential comes from the Q_{mp} function and appears in all the z integrals. Analytical expressions for the energy moments in the low-q limit could not be obtained, even for the double-step case. We could only infer that the first nonvanishing q-dependent term in the expansion of the dispersion relation $w(q)$ is proportional to q^2.

If $q=d=0$ is considered, the bulk plasma energy w_p is recovered in the limit $\tau\rightarrow 0$. The values used in the calculations are summarized in Table I. The last column of Table I is the experimental value of the monopole surface plasmon ($q=0$) used in the normalization of the experimental data given in Ref. 12.

In the case of Al, no polynomial approximation is given in Ref. 12. To obtain numerical results from the use of Eq. (31), a trial value of $\delta=1.6$ a.u. was used. No effective-mass-type correction was performed.

TABLE I. Physical parameters used in the calculations. δ and m^* for Na, K, and Cs are obtained from the fitting of our model [Eq. (32)] for surface plasmon and the polynomial approximation to the experimental data given in Ref. 12. The δ and m^* values for Al are trial values. d is the width of the electronic step (see text). The experimental surface-plasmon frequencies used in the normalization of the data reported in REf. 12 are also given.

	r_s	d	δ	m^*	w_{sp}(exp) (eV)
Al	2.07		1.6	1	10.3
Na	3.93	4.34	1.06	1.14	3.99
K	4.86		0.95	1.30	2.73
Cs	5.62		0.60	1.58	1.99

III. RESULTS AND DISCUSSION

We have applied the method described in the preceding section to free-electron-like plane surfaces. The first point in question is related to the value of the τ parameter that must be used, once q is fixed, in order to calculate the dispersion relation $w(q)$.

Figure 1 shows the contribution to the energy of the Coulomb $[\sqrt{m_3(C)/m_1}]$ and kinetic $[\sqrt{m_3(T)/m_1}]$ terms for Na at three different q values, as functions of the τ parameter. Whereas the kinetic contribution has a monotonic increasing behavior, the Coulomb term develops an abrupt increase for τ approximately equal to $2q$ (marked below by arrows). Though not apparent on the scale represented in Fig. 1, the Coulomb term shows an oscillatory behavior along the τ axis that resembles the structure obtained for the excitation energy of a metallic sphere as a function of q_r.[16] In this last case, the peaks of the oscillatory behavior of the energy function corre-

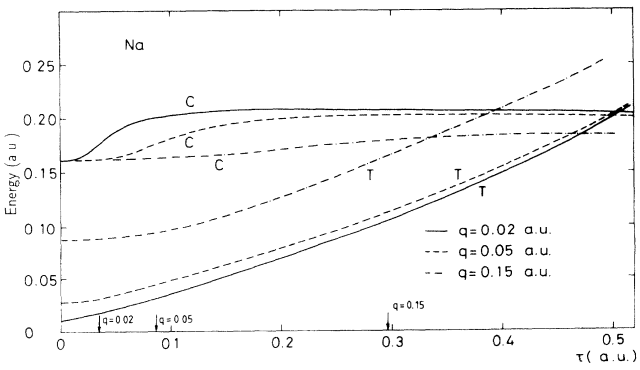

FIG. 1. τ dependence of the Coulomb (C) and kinetic (T) contributions to the excitation energy for Na. Curves labeled C are $\sqrt{m_3(C)/m_1}$ and those labeled T are $\sqrt{m_3(T)/m_1}$. Three different values of q are considered. The arrows below indicate the place of largest slope in each case. Equation (30) is used for the electronic profile.

spond with the q_r-quantized values that describe the bulk modes of the system. In the planar case, the first τ derivative of the total energy gives a much more accurate evaluation of the resonant values of τ, as can be seen in Fig. 9 (for $q=0.05$ a.u.), which will be commented on below (in addition to Na, results for Al, K, and Cs are also shown). This q-dependent resonant value is the one chosen in the determination of the energy of the modes. In Fig. 1, a double-step density is considered [Eq. (30)], whereas in Fig. 9 a soft profile is used [Eq. (31)]. Within the accuracy of our numerical calculations, the resonant value of τ does not depend on the electronic profile for these low q values, as is pointed out below.

As q increases, the resonant behavior becomes less and less apparent, as the Coulomb contribution is flatter and the kinetic term is shifted towards larger values, thus making the structure of the total energy less pronounced and in turn the mode less observable. This behavior agrees with experimental results that show that the multipole modes become unobservable for values of q much smaller than the Landau damping cutoff value given approximately by $q_c=w_p/v_F=0.90\sqrt{r_s}$ ($q_c=0.45$ a.u. for Na, v_F is the Fermi velocity). In a TDLDA calculation of the dispersion relation of the multipole modes given in Ref. 12, the error bars become larger for increasing values of q (see Figs. 6–8 therein) showing an increase in damping, in agreement with our results.

To give an idea of the sensitivity of the resonant τ value on the width of the step, two different values of d are chosen to study the behavior of the Coulomb contribution. Figure 2 shows that the value of τ that makes the most abrupt variation of the energy is the same for both values of d (the position of the arrow is the same in both cases). Even for $d=0$ (a one-step electronic profile), the Coulomb term would show an abrupt increase in τ and so a multipole mode, contrary to the result obtained by Bennet[1] who found within a hydrodynamical calculation that multipole modes are strongly dependent on the electronic profile, and appear only for a certain value of the decay length at the surface.

Figure 3 shows all the different contributions to the energy in order to study the relative importance of the exchange and correlation interactions within the local model used [Eqs. (26) and (27)]. For $\tau=0.1$ a.u., the exchange term is about 13% of the Coulombic plus the kinetic contributions, whereas the correlation term is only about 4%. Both terms are negative [the values presented in Fig. 3 are $-\sqrt{|m_3(\mathrm{ex})/m_1|}$ and $-\sqrt{|m_3(\mathrm{cor})/m_1|}$, respectively] and tend to lower the slope of the dispersion relation in a similar way as was previously reported for bulk plasmons (see Ref. 17). If nonlocal effects are considered in the exchange term, its contribution to the Coulombic part decreases but still produces a lower slope.[26] The inclusion of exchange and correlation makes the Coulomb interaction weaker, the electrons freer, and decreases the necessary energy to create a plasma oscillation. Equation (31) is used for the electronic profile.

To study the dependence of our results on the metallic density, in Fig. 4 a comparison between the dressed

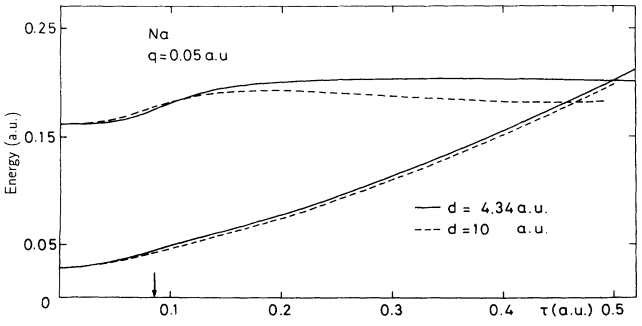

FIG. 2. Same as Fig. 1 for $q=0.05$ a.u. for two different values of the double-step width. The arrow below indicates the position of the largest slope for both cases.

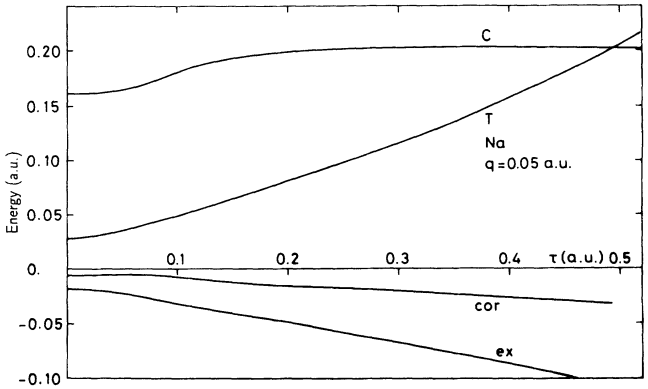

FIG. 3. Same as Fig. 1 for the Coulomb and kinetic contributions to the excitation energy, together with the exchange ($-\sqrt{|m_3(\mathrm{ex})/m_1|}$) and correlation ($-\sqrt{|m_3(\mathrm{cor})/m_1|}$) terms as functions of τ. Equation (31) is used for the electronic profile.

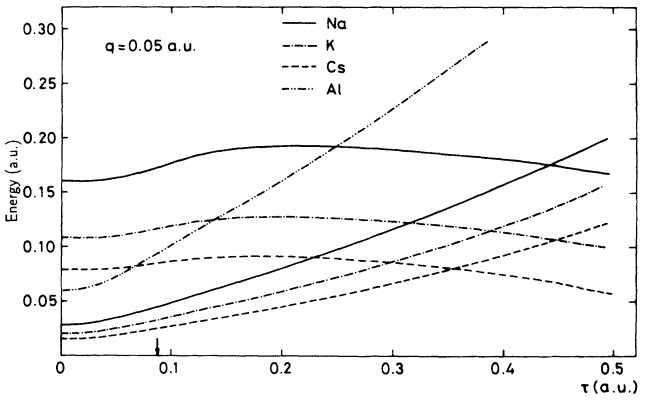

FIG. 4. Dressed Coulomb

$$(\sqrt{[m_3(C)+m_3(\mathrm{ex})+m_3(\mathrm{cor})]/m_1})$$

and kinetic (the same as in Fig. 1) contributions to the excitation energy as functions of τ for four different metals. The Coulombic term for Al is off the scale and crosses the kinetic branch for τ larger than 0.5 a.u. The arrow below indicates the position of the largest slope, the same in all cases.

Coulomb $(\sqrt{[m_3(C)+m_3(\mathrm{ex})+m_3(\mathrm{cor})]/m_1})$ and kinetic contributions for Al, Na, K, and Cs for a fixed value of $q=0.05$ a.u. is shown. The dressed Coulomb contribution of Al lies off the scale (it is about 0.45 a.u.) and crosses the kinetic branch for τ larger than 0.5 a.u. It is clear from the figure that the structure of the total energy is washed out as r_s is increased, as the cross point of the Coulombic and kinetic branches decreases, and the Coulomb contribution becomes flatter. This behavior again agrees with the tendency shown in the electron-loss spectra given in Ref. 12 (see Fig. 5 therein). The peak of the multipole mode is much less apparent in the Cs case than it is in Na or K. The transition from a collective to a single electron-hole excitation is related to the increasing contribution of the kinetic energy to m_3 and so to the position of the cross point of the Coulomb and kinetic branches, which decreases for higher r_s values. However, according to the above, Fig. 4 would predict the observability of multipole modes in Al, in contrast to experiments. This point will be discussed in the last section.

Figure 5 represents the dispersion relation for Na within a calculation that excludes exchange and correlation interactions and its aim is to compare the results obtained from the use of Eq. (30) (full line) and Eq. (31) (crosses). We also added the experimental data taken from Ref. 12. As was previously pointed out, there is a negligible dependence of the results on the details of the electronic profile for these values of q.

Figures 6–8 collect the full calculation [including exchange and correlation terms and using Eq. (31) for the electronic profile] of the dispersion relation for Na, K, and Cs (full curves). The best fit with experimental data takes place for K as was previously the case for monopolar surface modes.[19] The TDLDA results reported in Ref. 12 are also given. The bars in the figure indicate the uncertainty of these results. The extrapolation to $q=0$ of our numerical calculation gives a value of

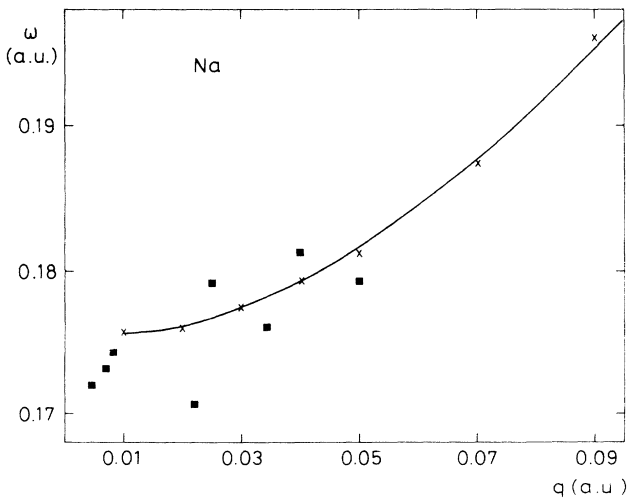

FIG. 5. Dispersion relation of multipole modes for Na. The solid line is obtained using a double-step profile [Eq. (30)] and the crosses using the soft profile [Eq (31)]. Exchange and correlation interactions are not included. Experimental data taken from Ref. 12 are also given (squares).

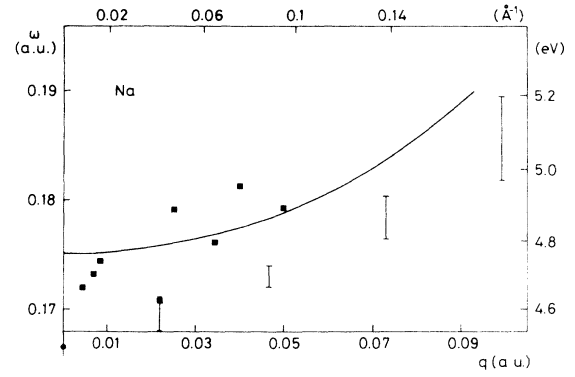

FIG. 6. Dispersion relation of the multipole plasmon modes for Na including exchange and correlation effects and using Eq. (31) for the electronic profile. Experimental data from Ref. 12 are included (squares). The vertical lines denote the results of the TDLDA calculation from Ref. 12. The dot at $q=0$ is the extrapolated plasma frequency in the TDLDA calculation.

$$w=\frac{w_p}{\sqrt{m^*}}a\ , \tag{34}$$

where m^* is the effective electronic mass and $a=0.84$ is independent of the metal, in excellent agreement with experimental findings.

As one moves from Na to Cs, the TDLDA results become better than the SR results. The reason lies in the nature of the SR method in which an average evaluation of the response function is implicit. As r_s increases, the electron-hole contribution to the average becomes more important as a consequence of the relative increase of the kinetic term as was discussed previously (see Fig. 4). The presence of electron-hole excitations lowers the average energy. Due to the energy factors in the SR [see Eqs. (3) and (8)], the high-energy collective state continues to exhaust the m_3 SR also at relatively high q, but not the m_1 SR, which begins to take contributions from single-particle excited states and then E_3 becomes lower than the TDLDA value.

Finally, Fig. 9 shows the first τ derivative of the total

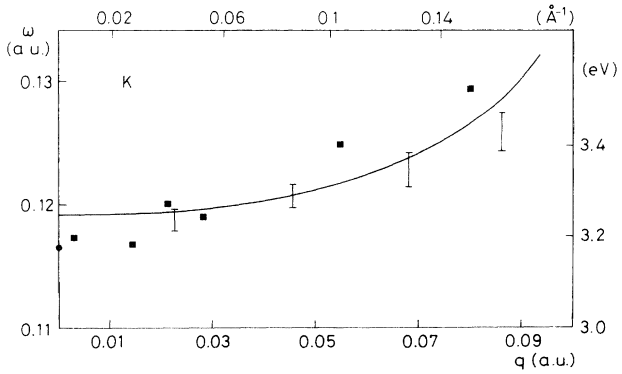

FIG. 7. Same as Fig. 6 for K.

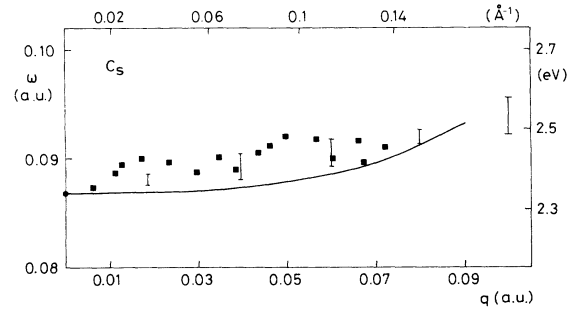

FIG. 8. Same as Fig. 6 for Cs.

energy which develops a pronounced peak for $\tau=2q$, nearly independent of the metal. Contrary to the findings of some previous works[1,27,28] that suggest that the multipole mode is a trapped standing wave inside the surface layer and therefore strongly dependent on the width of the surface region as a consequence of the matching condition, τ (and its associated wavelength $\lambda=2\pi/\tau$) is mainly determined by the localization of the operator $Q_{\rm mp}$ around $z=0$ determined by q in the exponential $e^{-q^2z^2}$. There are some arguments that support this observation. One is related to the behavior of the electronic-density fluctuation related to a multipole mode. In Ref. 12, the density distribution for $r_s=5$ a.u. and $q=0.06$ a.u. extends over a distance of about 16 a.u. on the z axis, while for this value of r_s the width of the surface region would be about 4 a.u. The other argument refers to a consequence of sum-rule calculations in that a relationship is established between the operator Q and the electronic-density fluctuation, which is, to first order in Q, given by Eq. (22),

$$n_1(\mathbf{r})=-\vec{\nabla}(n\vec{\nabla}Q)\ , \tag{35}$$

where n is the g.s. density. This relation gives to the n_1 function the same exponential dependence on z, that is to say, the plasma oscillation is localized in a region determined by q. There is, however, a residual dependence of τ on the metal that augments as q increases, thus making the localization region and the surface width comparable. The matching condition on τ determined by the width of the surface would give a constant value of τ for all q momenta and within a sum-rule calculation, it would produce a negative slope for the dispersion relation.

There are more resonant peaks for larger values of τ for a fixed q, however, they lie in the unobservable region due to the high value of the kinetic-energy contribution. Actually, the experimental values correspond to the first quantized value of τ (the one in Fig. 9). It is due to this quantization on the momentum along the z direction that makes it possible to obtain the dispersion relation of the multipole modes from inelastic-electron-scattering experiments in the reflection mode of Ref. 12 as there is no momentum conservation in the z direction.

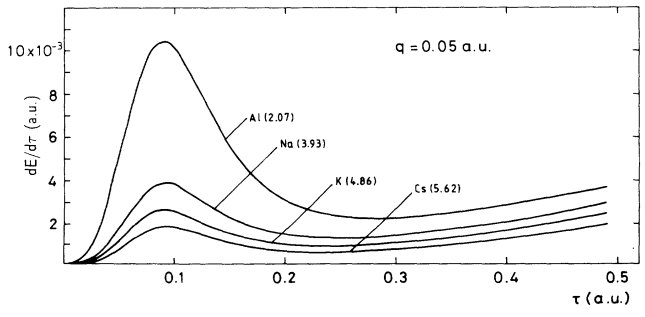

FIG. 9. First τ derivative of the excitation energy for four different metals as a function of τ. Exchange and correlation terms are included and a soft electronic profile is considered [Eq. (31)].

IV. CONCLUDING REMARKS

An alternative study which clarifies some aspects of multipole collective modes in metal surfaces is presented. The interplay between Coulomb and kinetic energies allows us to predict under what circumstances these modes might be observable. The Coulomb contribution develops resonant behavior for discrete values of the z-direction momentum. This resonant structure is washed out by the kinetic contribution for increasing q values smaller than the Landau damping cutoff. For a fixed q, only the first quantized mode turns out to be observable. The resonant z-direction momentum is approximately equal to $2q$ for low q values and is increasingly dependent on the surface profile as its associated wavelength becomes comparable to the surface size. Exchange and correlation effects reduce the slope of the dispersion relation due to the weakening of the Coulomb interaction.

The fact that in the case of Al experimental data do not show multipole modes means that further modifications to our calculations must be made in order to account for the probability of excitation of these modes. In Refs. 7 and 8 the imaginary part of the centroid function $d(w)$ directly related to the probability is obtained. This function develops a resonant structure at the multipole frequency, which decreases for denser metals. This tendency competes with the increasing resonant structure shown in Fig. 9. Considering that a simple metal in our model is characterized by three parameters r_s, δ, and m^*, everything tends to suggest that the softening of the electronic profile at the surface produces an effective strong damping mechanism that extinguishes the mode.

ACKNOWLEDGMENTS

We would like to thank J. Martorell for useful discussions. This work has been supported in part by the Comisión Asesora de Investigación Cientifica y Tecnica (CAICyT), Spain under Grant No. PB92-0761.

APPENDIX

In this appendix we summarize the formulas obtained for m_1 and m_3 using the operator $Q_{\rm mp}$ [Eq. (29)] for an arbitrary electronic density $n(z)$. The expressions are given per unit area in the XY plane. From a dimensional analysis, we have incorporated the effective electronic mass m^* to the energy expression $\sqrt{m_3/m_1}$ and have assigned it to the m_3 term. We obtain

$$m_1=\int_{-\infty}^{\infty}dz\,e^{-2q^2z^2}\{n[q^2+\tau^2+4q^4z^2][\cos(2\tau z)+1]+n'\tau\sin(2\tau z)\}\ , \tag{A1}$$

$$\begin{aligned}m_3(T)=&\frac{1}{3m^{*2}}\int_{-\infty}^{\infty}dz\,\sigma e^{-2q^2z^2}\{8q^2\tau\sin(2\tau z)[a_{11}z+a_{13}z^3]+\cos(2\tau z)[a_{20}+a_{22}z^2+a_{24}z^4]+a_{30}+a_{32}z^2+a_{34}z^4\}\\&+\frac{1}{4m^{*2}}\int_{-\infty}^{\infty}dz\,ne^{-2q^2z^2}\{4q^2\tau\sin(2\tau z)[b_{11}z+b_{13}z^3+b_{15}z^5]\\&+\cos(2\tau z)[b_{20}+b_{22}z^2+b_{24}z^4+b_{26}z^6]+b_{30}+b_{32}z^2+b_{34}z^4+b_{36}z^6\}\\&+\frac{1}{4m^{*2}}\int_{-\infty}^{\infty}dz\,n'e^{-2q^2z^2}\{\sin(2\tau z)[c_{10}+c_{12}z^2+c_{14}z^4]\\&+\cos(2\tau z)[c_{21}z+c_{23}z^3+c_{25}z^5]+c_{31}z+c_{33}z^3+c_{35}z^5\}\ ,\end{aligned} \tag{A2}$$

$$\begin{aligned}m_3(C)=&\frac{2\pi}{m^*}\int_{-\infty}^{\infty}dz\,ne^{-2q^2z^2}\\&\times\{\tau\sin(2\tau z)[q^2+\tau^2-12q^4z^2]+2q^2\cos(2\tau z)[(q^2+3\tau^2)z-4q^4z^3]+2q^2[(q^2-\tau^2)z-4q^4z^3]\}\\&\times\int_{-\infty}^{\infty}dz'(n-n_j)\mathrm{sgn}(z'-z)+\frac{4\pi}{m^*}\int_{-\infty}^{\infty}dz\,nn_je^{-2q^2z^2}\{4q^2\tau z\sin(2\tau z)+[4q^4z^22-\tau^2]\cos(2\tau z)+4q^4z^2+\tau^2\}\\&+\frac{4\pi q}{m^*}\int_{-\infty}^{\infty}dz\int_{-\infty}^{z}dz'n(z)n(z')e^{-q^2(z^2+z'^2)}e^{-q(z-z')}\\&\times\{2\tau q\sin[\tau(z-z')][q(z-z')+1]-2\tau q^2\sin[\tau(z+z')](z+z')\\&+\cos[\tau(z-z')][q^2-\tau^2-4q^4zz'+2q^3(z-z')+\cos[\tau(z+z')][q^2+\tau^2-4q^4zz'+2q^3(z-z')]\}\ ,\end{aligned} \tag{A3}$$

$$\begin{aligned}m_3(\mathrm{ex+cor})=&\frac{1}{3m^*}\int_{-\infty}^{\infty}dz\,e^{-2q^2z^2}\left[-\left[\frac{3}{\pi}\right]^{1/3}n^{1/3}+c\frac{gn^{2/3}+2n^{1/3}}{(gn^{1/3}+1)^3}\right]\\&\times(\cos(2\tau z)\{2q^2n'[3(q^2+\tau^2)z-4q^4z^3]+n[(3q^2+\tau^2)^2-24q^4(q^2+\tau^2)z^2+16q^8z^4]\}\\&+\sin(2\tau z)\{\tau n'[3q^2+\tau^2-12q^4z^2]+8q^2\tau n[-(3q^2+\tau^2)z+4q^4z^3]\}\\&-2q^2n'[(-3q^2+\tau^2)z+4q^4z^3]+n[(3q^2+\tau^2)^2+8q^4z^2(-3q^2+\tau^2)+16q^8z^4)\ ,\end{aligned} \tag{A4}$$

where

$$\sigma=\tfrac{3}{5}(3\pi^2)^{2/3}n^{5/3}+\frac{\beta}{4}\frac{n'^2}{n}\ , \tag{A5}$$

$$\begin{aligned}&a_{11}=q^2-\tau^2\ ,\quad a_{13}=4q^4\ ,\quad a_{20}=13q^4-2q^2\tau^2+\tau^4\ ,\quad a_{22}=8q^4(q^2-3\tau^2)\ ,\quad a_{24}=16q^8\ ,\\&a_{30}=13q^4+20q^2\tau^2+3\tau^4\ ,\quad a_{32}=8q^4(q^2+2\tau^2)\ ,\quad a_{34}=16q^8\ ,\end{aligned} \tag{A6}$$

$$\begin{aligned}&b_{11}=43q^4+26q^2\tau^2+3\tau^4\ ,\quad b_{13}=-8q^4(13q^2+5\tau^2)\ ,\quad b_{15}=48q^8\ ,\quad b_{20}=9q^6-43q^4\tau^2-13q^2\tau^4-\tau^6\ ,\\&b_{22}=4q^4(43q^4+78q^2\tau^2+15\tau^4)\ ,\quad b_{24}=-16q^8(13q^2+15\tau^2)\ ,\quad b_{26}=64q^{12}\ ,\\&b_{30}=9q^6+55q^4\tau^2+15q^2\tau^4+\tau^6\ ,\quad b_{32}=4q^4(43q^4+2q^2\tau^2+3\tau^4)\ ,\quad b_{34}=-16q^8(13q^2-3\tau^2)\ ,\quad b_{36}=64q^{12}\ ,\end{aligned} \tag{A7}$$

$$\begin{aligned}&c_{10}=-2\tau^5-26q^4\tau-12q^2\tau^3\ ,\quad c_{12}=114q^6\tau+80q^4\tau^3\ ,\quad c_{14}=-160q^8\tau\ ,\\&c_{21}=-52q^6-72q^4\tau^2-20q^2\tau^4\ ,\quad c_{23}=96q^8+160q^6\tau^2\ ,\quad c_{25}=-64q^{10}\ ,\\&c_{31}=-52q^6-32q^4\tau^2-12q^2\tau^4\ ,\quad c_{33}=96q^8-64q^6\ ,\quad c_{35}=-64q^{10}\ ,\end{aligned} \tag{A8}$$

$$c=-\frac{0.88}{3}\left[\frac{4\pi}{3}\right]^{1/3}\ ;\quad g=\frac{7.8}{m^*}\left[\frac{4\pi}{3}\right]^{1/3}\ ;\quad n_j=n_0\theta(-z)\ . \tag{A9}$$

[1]J. Bennet, Phys. Rev. B **1**, 203 (1970).
[2]J. Harris and A. Griffin, Can. J. Phys. **48**, 2592 (1970).
[3]A. Eguiluz and J. J. Quinn, Phys. Lett. **53A**, 151 (1973).
[4]J. E. Inglesfield and E. Wikborg, J. Phys. C **6**, L158 (1973).
[5]B. B. Dasgupta, Z. Phys. B **29**, 245 (1978).
[6]J. F. Dobson and G. H. Harris, J. Phys. C **21**, L729 (1988).
[7]P. J. Feibelman, Prog. Surf. Sci. **12**, 287 (1982).
[8]A. Liebsch, Phys Rev. B **36**, 7378 (1987).

[9]H. J. Levinson, E. W. Plummer, and P. J. Feibelman, Phys. Rev. Lett. **43**, 952 (1979).
[10]J. Monin and G. A. Boutry, Phys. Rev. B **9**, 1309 (1974).
[11]K.D. Tsuei, E. W. Plummer, A. Liebsch, K. Kempa, and P. Bakshi, Phys. Rev. Lett. **64**, 44 (1990).
[12]K. D Tsuei, E. W. Plummer, A. Liebsch, E. Pehlke, K. Kempa, and P. Bakshi, Surf. Sci. **247**, 302 (1991).
[13]G. Bertsch and W. Ekardt, Phys. Rev. B **32**, 7659 (1985).
[14]M. Brack, Phys. Rev. B **39**, 3533 (1989).
[15]Ll. Serra, F. Garcias, M. Barranco, J. Navarro, C. Balbás, and A. Mañanes, Phys. Rev. B **39**, 8247 (1989).
[16]Ll. Serra, F. Garcias, M. Barranco, N. Barberán, and J. Navarro, Phys. Rev. B **41**, 3434 (1990).
[17]Ll. Serra, F. Garcias, M. Barranco, N. Barberán, and J. Navarro, Phys. Rev. B **44**, 1492 (1991).
[18]Ll. Serra, F. Garcias, J. Navarro, N. Barberán, M. Barranco, and M. Pi, Phys. Rev. B **46**, 9369 (1992).
[19]N. Barberán, J. Sellarès, and J. Bausells, Surf. Sci. **292**, 159 (1993).
[20]O. Bohigas, A. M. Lane, and J. Martorell, Phys. Rep. **51**, 267 (1979).
[21]E. Lipparini and S. Stringari, Phys Rep. **175**, 103 (1989).
[22]J. Navarro and M. Barranco, Nucl. Phys. A **505**, 173 (1989).
[23]S. H. Vosko, L. Wilk, and M. Nusair, Can. J. Phys. **58**, 1200 (1980).
[24]J. P. Perdew and A. Zunger, Phys. Rev. B **23**, 5048 (1981).
[25]E. Lipparini and F. Pederiva, Z. Phys. D **22**, 553 (1992).
[26]J. Providencia, Jr. and N. Barberán, Phys. Rev. B **45**, 6935 (1992).
[27]C. Schwartz and W. L. Schaich, Phys. Rev. B **26**, 7008 (1982).
[28]C. Schwartz and W. L. Schaich, Phys. Rev. B **30**, 1059 (1984).